SCIENCE CHINA Materials ARTICLES

mater.scichina.com link.springer.com

Published online 4 February 2021 | https://doi.org/10.1007/s40843-020-1565-8
Sci China Mater 2021, 64(7): 1679–1686

Ultrafast photoinduced strain in super-tetragonal $PbTiO_3$ ferroelectric films

Linxing Zhang[1†*], Darui Sun[2†], Maosheng Chai[3], Xianran Xing[4], Jun Chen[5], Bingbing Zhang[2,6*] and Jianjun Tian[1*]

ABSTRACT **The ultrafast photoinduced strain (UPS) resulting from the coupling of piezoelectric and photovoltaic effects in ferroelectric has been focused in the last decade, endowing them with extensive applications including ultrafast optical memories, sensors and actuators with strain engineering. The mechanism of screening of the depolarization field by photoinduced carriers is generally accepted for UPS in ferroelectrics, while the thermal component of the strain is usually diluted as the offset and has not been systematically confronted, leading to unnecessary confusion. Herein, both the positive and negative thermal expansion effects in composite ferroelectric epitaxial films are investigated by use of high-repetition-rate ultrafast X-ray diffraction, along with the piezoelectric and photovoltaic effects. The coupling of the positive/negative thermal effects and the piezoelectric/photovoltaic effects in ultrafast strain is evidenced and can be regulated. The opposite lattice responses due to different thermal effects of the samples with different axial ratios are observed. The maximum UPS is up to 0.24%, comparable to that of conventional ferroelectric. The interaction between the thermal and ferroelectric effects in the induced strain could promote the diversified applications with the coupling of light, heat and electricity.**

Keywords: ferroelectrics, epitaxial films, piezoelectric and photovoltaic, thermal effect

INTRODUCTION

Ferroelectric has been discovered as a smart functional material for nearly a hundred years [1], which possesses the spontaneous polarization that can reverse under an external electric field. The coupling of two or more properties in ferroelectric materials promotes their extensive applications, such as multiferroic, ferroelectric photovoltaic, and ferroelectric resistivity [2–4]. Recently, ultrafast photoinduced strain (UPS) that combines the piezoelectric and photovoltaic effects (PP effects) has been explored in ferroelectric thin films of $PbTiO_3$ (PTO) and $BiFeO_3$ in the last decade which is ascribed to the screening of the depolarization field by photoinduced carriers [5–8]. The UPS effects extend their applications in ultrafast strain engineering and optical actuation devices. The strain deformation and gradient can be up to on the order of 0.5% and 10^6 m^{-1}, respectively, at picosecond timescale [5,6,9]. The research of ferroelectric UPS is of growing interest. The lattice expansion of UPS can shift the relative free energies of different phases and induce a transient reversible transformation from a state of coexisting tilted tetragonal-like and rhombohedral-like phases to an untilted tetragonal-like phase in $BiFeO_3$ thin films [8]. Both the magnitude and sign (contraction and expansion) of the UPS deformation can be tuned by the polarization state through the prepoling, deriving from the internal electric field (imprint field and depolarization field) [10], which is different to the other photoinduced mechanisms such as thermal elasticity [11], electrostriction [12], and charge transfer [13].

Light-matter interaction would cause both non-thermal

[1] Institute for Advanced Materials and Technology, University of Science and Technology Beijing, Beijing 100083, China
[2] Beijing Synchrotron Radiation Facility, Institute of High Energy Physics, Chinese Academy of Sciences, Beijing 100049, China
[3] Center for Nano and Micro Mechanics, Tsinghua University, Beijing 100084, China
[4] Beijing Advanced Innovation Center for Materials Genome Engineering, Department of Physical Chemistry, University of Science and Technology Beijing, Beijing 100083, China
[5] School of Mathematics and Physics, University of Science and Technology Beijing, Beijing 100083, China
[6] University of Chinese Academy of Sciences, Beijing 100049, China
[†] These authors contributed equally to this work.
[*] Corresponding authors (emails: linxingzhang@ustb.edu.cn (Zhang L); zhangbb@ihep.ac.cn (Zhang B); tianjianjun@mater.ustb.edu.cn (Tian J))

and thermal lattice responses in the same material, since the photon energy of laser would transfer to the lattice through the electron-phonon interaction and induce a temperature increase, resulting in the strain of lattice. Most materials have positive thermal expansion coefficient, such as Al alloys [14] and ferroelectric $BiFeO_3$ [15], while some unique materials have negative thermal expansion coefficient, such as ZrW_2O_8 and PTO [15]. In the $BiFeO_3$ systems, the heating effect was firstly confronted by Wen *et al.* [6]. The total photoinduced strain including PP effects-induced strain within 2 ns and positive thermal expansion in tens of nanoseconds has been distinguished. However, in the negative thermal expansion systems of PTO or $Pb(Zr_xTi_{1-x})O_3$ (PZT), the thermal effects have not been investigated to be responsible for the lattice contraction [5,10]. The small compressive strain caused by the negative thermal effect would be overcompensated by the large expansion induced by ferroelectric polarization. Hence, it is significant to distinguish the photovoltaic and thermal effects in systems with both positive and negative expansion coefficients. With insight into the coupling effect of them, there would be multiple levels of strain that can be regulated. Here, we investigate two kinds of UPS of PTO composite films, which indicate the coupling of the positive/negative expansion and the PP effects-induced strain. In-depth understanding of the combined effect of thermal effect and PP effects-induced strain could help regulate the coupling application of the UPS.

EXPERIMENTAL SECTION

The films were grown by the radio-frequency (rf) magnetron sputtering. The target with 10% excess PbO was sintered at 1100°C for 2 h. The deposition system was firstly pumped to a prepared pressure up to 10^{-6} Torr with the substrate heated at 575–625°C, which was the deposition temperature. The deposition gas included argon and oxygen. Different gas ratios can cause changes in composition, that is 10% O_2 for PT(II) and 0% O_2 for PT(I) (the Pb/Ti of PT(II) and PT(I) are about 1.29 and 3.24, respectively). The grown pressure was kept at 9 mTorr during the deposition. A pre-sputtered process was carried out to clean the surface of target for 20 min. The films were grown with the rf power of 110 W. After deposition, the film was annealed for 30 min at the deposition temperature and atmosphere, and then cooled down to room temperature at 5°C min^{-1}. The crystal structure of the film was investigated using X-ray diffraction (XRD), which was performed at Beijing Synchrotron Radiation Facility (1W1A beamline, China) with high-resolution synchrotron X-ray, and the diffractometer (PW3040/60, PANalytical, Holland) with Cu Kα radiation. The piezoresponse force microscopy (PFM) was examined by Asylum Research MFP-3D-Infinity with Olympus AC240TM Pt/Ti-coated silicon cantilevers (Asylum Research, USA). The ultrafast XRD (UXRD) measurements were carried out on the UXRD setup implemented at 1W2B beamline of Beijing Synchrotron Radiation Facility with picosecond time resolution. The detailed procedure is described in the next section.

RESULTS AND DISCUSSION

We devise the new ferroelectric of PTO/PbO composite epitaxial film to study UPS due to its strong ferroelectric and newfound ferromagnetic characteristic [16,17]. The PTO and PbO with similar crystalline structures can be grown into the single-lattice-parameter epitaxial film through the method of "interphase strain", as shown in the crystalline structure schematic (Fig. 1a). The material of PTO with a small lattice is inevitably subjected to the tensile stress from the material of PbO with a large lattice, thereby introducing a large lattice strain. Hence the structure of PTO can be elongated by the strain from PbO. The samples were obtained under the similar condition as in our previous report [16], which demonstrates different compositions of PTO/PbO for PT(I) and PT(II). The synchrotron-based out-of-plane XRD demonstrates the different single *c* lattice parameters for PT(I) and PT(II) (Fig. 1b). Combined with the in-plane scans (not shown here), PT(I) has a larger axial ratio (*c*/*a*) of 1.235 than that of 1.142 for PT(II), which is ascribed to the higher content of PbO in PT(I) resulting in larger interphase strain than that of PT(II). As reported ferroelectric properties, both PT(I) and PT(II) possess the large remanent polarization, i.e., higher than 230 and 120 μC cm^{-2}, respectively [16]. Hereby, we carried out the PFM to assist in proving their ferroelectric (Fig. 1c–f). The three-dimensional (3D) images combine with the morphology image in terms of height and out-of-plane amplitude or phase image in terms of color. The contrast of amplitude and phase is obviously different to the morphology, indicating the characteristic of ferroelectric domain for both PT(I) and PT(II). The value of amplitude in PT(II) is larger than that in PT(I), which would be ascribed to the smaller axial ratio resulting in the easy switching of domain in PT(II). More importantly, the thermal expansion of the two films can be controlled from negative to positive by the composition of PTO and PbO, which will be discussed in detail below.

The UXRD measurements were performed on the PTO

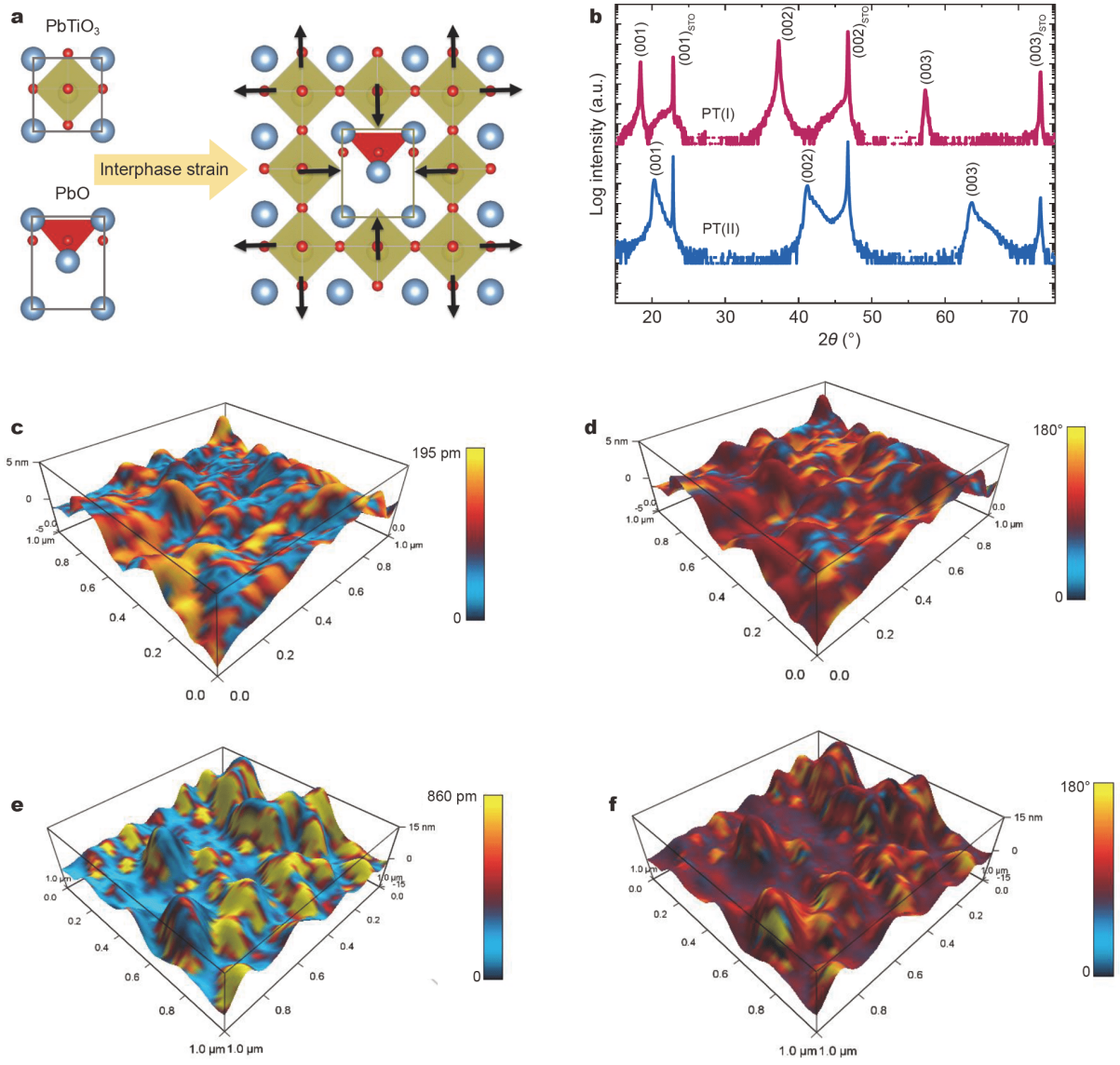

Figure 1 (a) Schematic of interphase strain for forming super-tetragonal structure of present thin films. (b) Synchrotron-based out-of-plane XRD of PT(I) and PT(II) epitaxial thin films on (100) STO substrates. (c, d) 3D PFM image of morphology and out-of-plane amplitude and phase image in PT(I) films, respectively. (e, f) 3D PFM image of morphology and out-of-plane amplitude and phase image in PT(II) films, respectively.

composite film on the UXRD setup implemented at 1W2B beamline of Beijing Synchrotron Radiation Facility with picosecond time resolution [18]. The 300-fs laser pulses from the high-repetition-rate fiber laser system (Tangerine HP, Amplitude Systems) at a repetition rate of 19.2 kHz were used to illuminate the sample at an incident angle of 45° within an elliptical footprint of 970 μm × 400 μm full width half maximum (FWHM). The optical excitations were provided by the third-harmonic generation (3.62 eV) of the laser system, beyond the bandgap of the sample. The monochromatic X-ray beam (energy resolution ($\Delta E/E$) ~0.01%) at a photon energy of 10 keV was focused into a 72-μm FWHM spot center in the optically illuminated area, by use of the poly-capillary lens. The high-repetition-rate laser pulses were synchronized to the timing signal from the storage ring and the time delay between the laser and X-ray pulse was controlled by the programmable delay line. The probed X-ray pulses at different time delays after the laser pulses were then gated out by a 2D area detector (Pilatus 100k, Dectris), as shown schematically in Fig. 2a.

The diffraction intensity distribution of the PT(II)

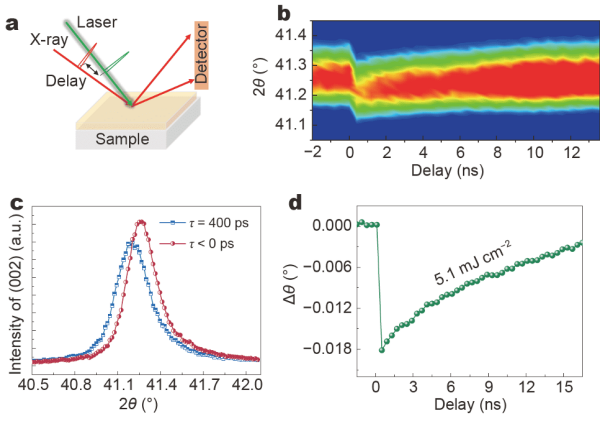

Figure 2 (a) Schematic of the time-resolved XRD experiment. (b) 2D diagram of the diffraction intensity distribution of (002) Bragg peak of PT(II) as a function of time delay, upon the excitation by the 3.62 eV laser pulses at the fluence of 5.1 mJ cm^{-2}. (c) The θ-2θ scans of (002) reflection before (τ < 0) and after (τ = 400 ps) laser excitation. (d) Angular shift of (002) peak as a function of time delay.

(002) reflection was measured after the laser excitation at the fluence of 5.1 mJ cm^{-2}, as a function of delay time, which is drawn in 2D diagram as shown in Fig. 2b. An apparent out-of-plane expansion was observed upon photoexcitation, resulting in a shift of the (002) reflection of PT(II) to lower Bragg angle, as shown in Fig. 2c. The photoinduced strain ($\Delta c/c$) reaches its maximum of 0.14% at 400 ps time delay (τ), along with a slight Bragg peak broadened from 0.246° to 0.275°. The intensity of the reflection decreases after photoexcitation, which could be ascribed to the strain gradient arising from the inhomogeneous spatial profile or from localized lattice distortion [6,7]. The angular change of the PT(II) (002) reflection as a function of pump-probe delay is shown in Fig. 2d, exhibiting the apparent UPS in present ferroelectric systems. The UPS in ferroelectrics was well studied and can be mainly ascribed to the PP effects due to the screening of depolarization field by the photoinduced carriers [5,6], in accordance with the photoinduced expansion observed in our experiment at the given time scale.

To systematically illustrate the factors of UPS, the role of thermal expansion in ferroelectrics needs to be carefully addressed. Through the utilization of high-repetition-rate laser system, the huge stationary thermal gradient was introduced. The ultrafast dynamics observed in a UXRD experiment at high repetition rate is usually superimposed on a large positive static temperature platform. The heating effect can be confirmed by static angular shift ($\Delta\theta_s$), the difference of lattice parameter between the signals at negative pump-probe delays (τ < 0) and when laser is off for a long time such as several minutes (turn-off state), which is usually offset in the transient angular shift ($\Delta\theta_t$). The interval between successive excitation pulses is 52 μs in the present 19.2 kHz laser, and hence the state at τ < 0 is roughly identical to the state at 52 μs after laser pulse.

Generally, the static temperature platform induces a positive thermal expansion in most of the ferroelectric materials. Here in our experiments, we observed both the negative and positive thermal expansion in different composite PTO samples (Fig. 3). The blue triangles represent the diffraction signals at laser turn-off state that is as a reference, while the green circles and red squares denote the peak shifts from negative time delay (τ < 0) to the positive delay up to 10 ns (Fig. 3a, b). As shown in Fig. 3a, the state at τ < 0 has a higher value than that at the turn-off case (a positive angular shift) in PT(II) sample, whereas the state at τ < 0 in PT(I) is lower than that at the turn-off case (a negative angular shift) (Fig. 3b), indicating a negative thermal expansion in PT(II), while a positive thermal expansion in PT(I). However, the state after laser pulse (τ = 400 ps) of both PT(II) and PT(I) present the negative angular shift relative to the state of both turn-off and before laser pulse (τ < 0), indicating the positive lattice expansion due to the PP effects of the depolarization field, which is similar to the above result in Fig. 2.

The direct evidences can also be observed in the θ-2θ scans of PT(II) and PT(I) (002) Bragg reflection. The state before (τ < 0) Bragg angle of PT(II) has a higher value than that at the turn-off state, whereas the state before (τ < 0) Bragg angle of PT(I) has a lower value than that at the turn-off state. This also indicates the PT(II) presents a negative thermal expansion, while the PT(I) shows a positive thermal expansion, consistent with the results of the angular shift of delay time.

To understand the complex dynamics of both depolarization effect and thermally induced responses, we carried out the analysis of delay process. The Bragg reflection intensities at different delay times were divided by the intensity without laser excitation for a long time (turn-off), and the positions at the high-angle and low-angle sides of the reflection center were taken, respectively, as shown in Fig. 3e, f. In the PT(II) systems, the value of high-angle side increases, while that of the low-angle side decreases, and then both trend to 1 and cross at the time of about 2.5 ns, indicating a state similar to laser off. This is consistent with the decay within about 2 ns of positive lattice strain by the depolarization effect along

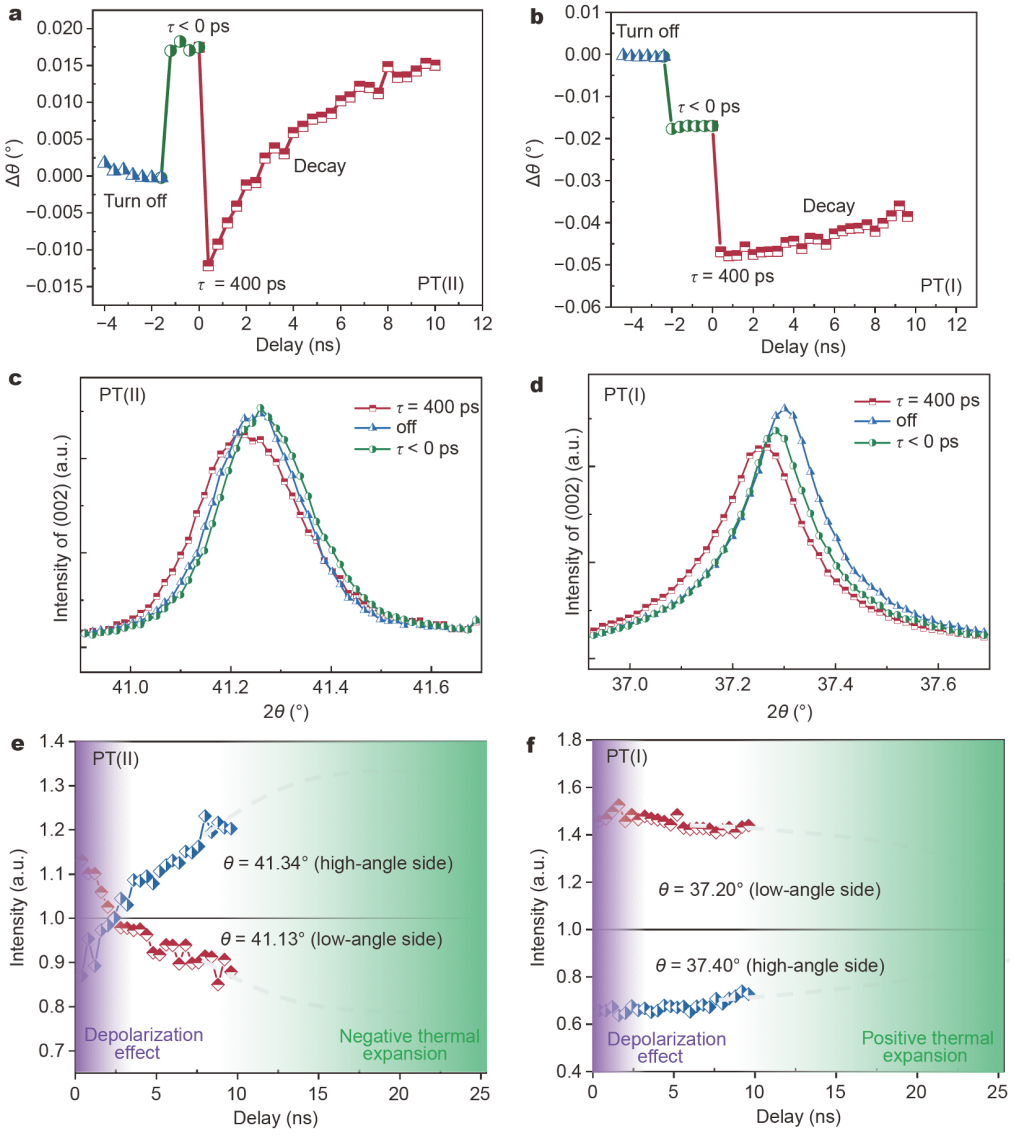

Figure 3 (a, b) Angular shift of PT(II) and PT(I) (002) Bragg reflection, respectively, as a function of delay time at the different states: turn-off, before ($\tau < 0$) and after ($\tau \geq 400$ ps). (c, d) The θ-2θ scans of PT(II) and PT(I) (002) Bragg reflection, respectively, at the different states: turn-off, before ($\tau < 0$) and after ($\tau = 400$ ps). (e, f) The intensity of the low- and high-angle sides of PT(II) and PT(I) (002) Bragg reflection divided by the turn-off state, respectively, as a function of delay time. The dotted line is a reference to possible trends, as a guide to the eye.

with carrier dynamics [6]. Subsequently, they separated from the cross point for more than 10 ns, demonstrating a long-lived decay process expected from heating of the ferroelectric. In contrast, for the PT(I) system, the cross point cannot be observed during the whole decay process. This can be ascribed to that the strains induced by both thermal and depolarization effect are positive expansion, resulting in difficulty in distinguishing the two decay processes. It is impossible to quickly return to the state of turn-off in the PT(I) systems.

To verify the role of the thermal and PP effects, we characterized the dependence of the UPS on the magnitude of the laser excitation. As shown in Fig. 4, the angular shifts of the 002 Bragg peak for PT(II) and PT(I) at different states of $\tau < 0$ ($\Delta\theta_s$) and at $\tau = 400$ ps ($\Delta\theta_t$) as a function of the pump fluence were measured. The state of turn-off was collected at a few points as a ground state with a constant value around zero shift for both PT(II) and PT(I). A linear fluence dependence of structural distortion at both states was observed. For both PT(I) and PT(II) samples, the $\Delta\theta_t$ ($\tau = 400$ ps) values exhibit the same negative dependence on the increasing incident

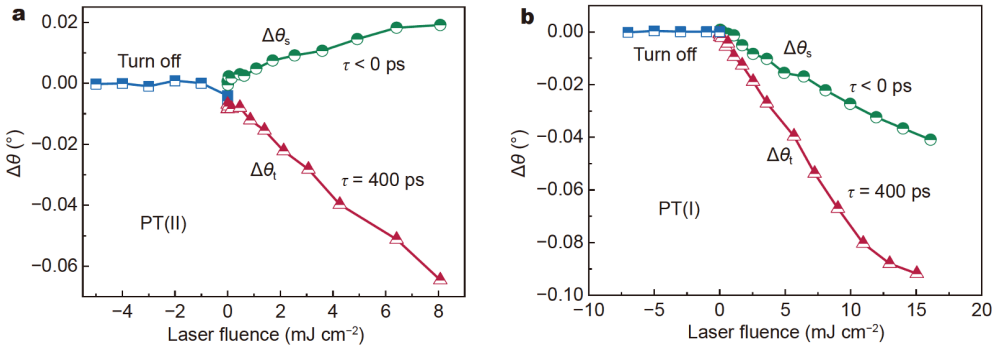

Figure 4 (a, b) Angular shift as a function of the laser fluence at different states of PT(II) and PT(I) at $\tau < 0$) and $\tau = 400$ ps, respectively. The state of turn-off is as a reference.

fluence, in correspondence to a lattice expansion due to the coupling of thermal effect and PP effects. However, the $\Delta\theta_s$ ($\tau < 0$) exhibits a positive dependence in PT(II), but a negative dependence in PT(I), demonstrating the opposite lattice response due to the thermal effect. As the state at $\tau < 0$ can be identical to the state at 52 μs after laser pulse, the PP effects can be ignored at this state. As we know, the static temperature platform can increase with the increasing pump fluence due to the accumulated heat of the high average power of laser pulses. Hence, the increasing contraction caused by the negative thermal effect is observed in the PT(II), while that is increasing expansion caused by the positive thermal effect in PT(I). Furthermore, at $\tau = 400$ ps, the increasing lattice expansion with the increasing incident fluence indicates that the increasing expansion of PP effects is higher than the increasing contraction of thermal effect in PT(II). This clearly illustrates the distinction between positive/negative thermal expansion and depolarization effects. The strain ($\Delta c/c$) can reach 1.5×10^{-3} for a laser fluence of 8.1 mJ cm^{-2} from the state of turn-off to after ($\tau = 400$ ps) excitation for both PT(II) and PT(I). The maximum strain can be up to 2.4×10^{-3} for a laser fluence of 15 mJ cm^{-2} for PT(I), which is comparable to the results of similar ferroelectric [6]. The large strain would be ascribed to the large polarization in present films, which would have large transient electric field resulting in PP effects.

To further demonstrate the different thermal effects in PT(II) and PT(I) samples, we performed the temperature-dependent XRD measurements. Fig. 5a shows the evolution of out-of-plane lattice parameter in terms of temperature, indicating the positive thermal expansion coefficient (2.83×10^{-5}°C^{-1}) in PT(I) and the negative coefficient (-1.99×10^{-5}°C^{-1}) in PT(II), consistent with our UXRD results. The thermal expansion properties of the present films with different axial ratios are related to their components of PbO and $PbTiO_3$. The repeated 19.2 kHz laser under the period of 52 μs with 10^6 cycles will cause a noticeable heat as discussed above (Fig. 5b). To speculate the mechanism of the UPS dependent on the time delay, we modeled the process by combining the thermal effect and the carrier-induced depolarization effect (Fig. 5c, d). The thermally induced strain of the green curves indicates a contracted strain for PT(II) and an expanded strain for PT(I). The red curves are the carrier-induced strains, which are expanded for both PT(II) and PT(I). The black curve is the sum of carrier-induced and thermally induced strain that represents the overall induced strain after photoexcitation. The shape of total strain for PT(I) is similar to that of previous report [6]. The expansion decreases as the delay increases. However, the total strain for PT(II) firstly decreases to a minimum value and then increases, which is ascribed to that the decline of positive (carrier-induced strain) expansion is faster than that of negative (thermally induced strain) expansion. The representative angular shift in PT(II) as a function of time delay demonstrates the contraction relative to the state at $\tau < 0$ during the delay process of 10–20 ns as shown in the inset of Fig. 5c. This trend confirms our conjecture that it is the same as the black line of overall induced strain, and that does not occur in thermal positive expansion materials. Schematic diagram of the whole process of PT(II) including carrier-induced strain and thermally induced negative strain is the same as shown in the test process in Fig. 5b (bottom curve).

CONCLUSIONS

We firstly observed the UPS in the new ferroelectric of PTO/PbO composite epitaxial films, whose tetragonality and polarization can be controlled by the interphase strain. The synchrotron-based UXRD with femtosecond

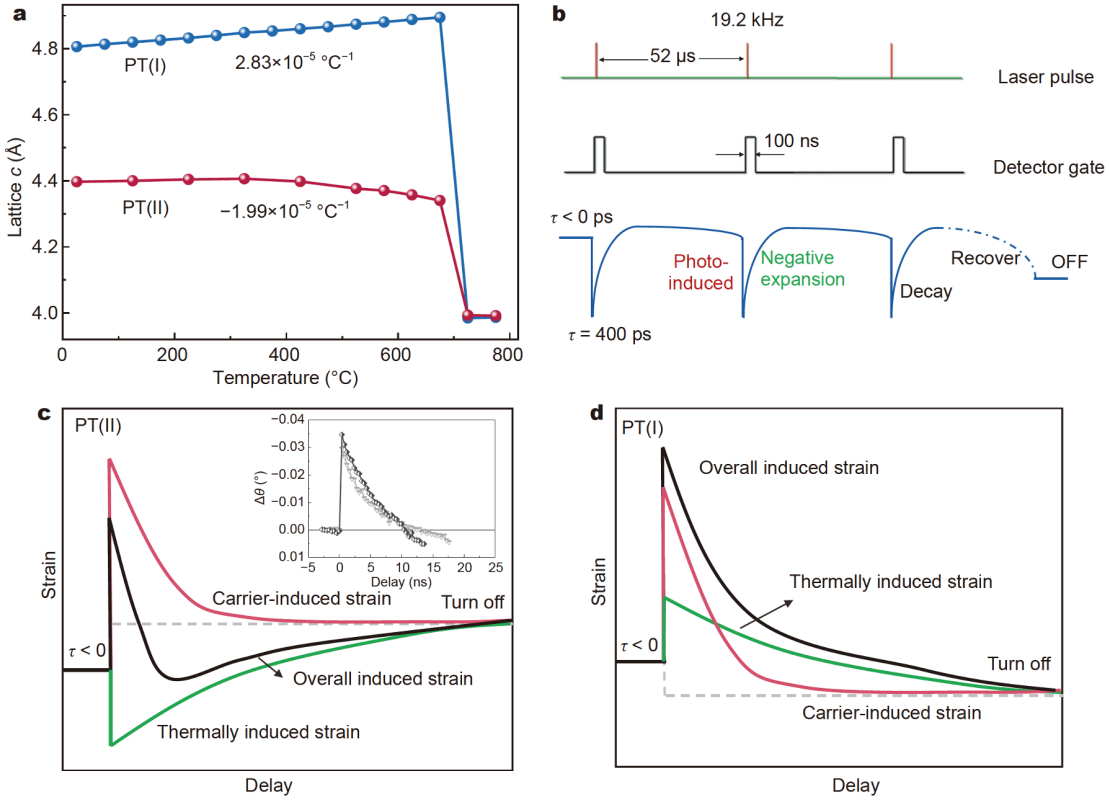

Figure 5 (a) The out-of-plane lattice parameter dependence on the temperature, indicating the negative thermal expansion in PT(II) and the positive thermal expansion in PT(I). (b) Sketch of the detection gate structure and strain evolution of PT(II). (c, d) Schematic for decomposition of the overall structural distortion into depolarization effect and thermal contributions of PT(II) and PT(I), respectively. The inset of (c) shows the representative angular shift of films (002) peak in PT(II) as a function of time delay.

pump laser pulses was utilized. The thermal effects of both negative and positive expansion coefficients were regulated in the UPS coupling with the piezoelectric/photovoltaic effects. PT(II) films with a negative coefficient (-1.99×10^{-5} °C^{-1}) demonstrate an expansion lattice before the delay time of about 2.5 ns, while a contraction lattice from 2.5 to 10 ns. The contraction lattice due to negative thermal effect in PT(II) increases with the increasing incident fluence, but an increasing expansion lattice is due to positive thermal effect for PT(I), indicating the opposite lattice response due to the thermal effect. The coexistence of different competitive thermal and photocarrier-induced depolarization effects in composites with different axial ratios provides a route to regulate and explore the functional properties in the multi-excitation environment.

Received 16 October 2020; accepted 16 November 2020; published online 4 February 2021

1 Valasek J. Piezo-electric and allied phenomena in Rochelle salt. Phys Rev, 1921, 17: 475–481
2 Wang J, Neaton JB, Zheng H, *et al.* Epitaxial $BiFeO_3$ multiferroic thin film heterostructures. Science, 2003, 299: 1719–1722
3 Guo R, You L, Zhou Y, *et al.* Non-volatile memory based on the ferroelectric photovoltaic effect. Nat Commun, 2013, 4: 1990
4 Rodrıguez Contreras J, Kohlstedt H, Poppe U, *et al.* Resistive switching in metal-ferroelectric-metal junctions. Appl Phys Lett, 2003, 83: 4595–4597
5 Daranciang D, Highland MJ, Wen H, *et al.* Ultrafast photovoltaic response in ferroelectric nanolayers. Phys Rev Lett, 2012, 108: 087601
6 Wen H, Chen P, Cosgriff MP, *et al.* Electronic origin of ultrafast photoinduced strain in $BiFeO_3$. Phys Rev Lett, 2013, 110: 037601
7 Schick D, Herzog M, Wen H, *et al.* Localized excited charge carriers generate ultrafast inhomogeneous strain in the multiferroic $BiFeO_3$. Phys Rev Lett, 2014, 112: 097602
8 Ahn Y, Pateras A, Marks SD, *et al.* Nanosecond optically induced phase transformation in compressively strained $BiFeO_3$ on $LaAlO_3$. Phys Rev Lett, 2019, 123: 045703
9 Li Y, Adamo C, Chen P, *et al.* Giant optical enhancement of strain gradient in ferroelectric $BiFeO_3$ thin films and its physical origin. Sci Rep, 2015, 5: 16650
10 Matzen S, Guillemot L, Maroutian T, *et al.* Tuning ultrafast photoinduced strain in ferroelectric-based devices. Adv Electron Mater, 2019, 5: 1800709
11 Schick D, Herzog M, Bojahr A, *et al.* Ultrafast lattice response of

photoexcited thin films studied by X-ray diffraction. Struct Dyn, 2014, 1: 064501
12 Chroneos A, Bracht H. Diffusion of n-type dopants in germanium. Appl Phys Rev, 2014, 1: 011301
13 Zhang B, He X, Zhao J, *et al.* Giant photoinduced lattice distortion in oxygen vacancy ordered $SrCoO_{2.5}$ thin films. Phys Rev B, 2019, 100: 144201
14 Alberts HL, Lourens JAJ. Thermal-expansion and elastic constants of dilute Cr-Al alloys. Phys Rev B, 1984, 29: 5279–5285
15 Chen J, Hu L, Deng J, *et al.* Negative thermal expansion in functional materials: Controllable thermal expansion by chemical modifications. Chem Soc Rev, 2015, 44: 3522–3567
16 Zhang L, Chen J, Fan L, *et al.* Giant polarization in super-tetragonal thin films through interphase strain. Science, 2018, 361: 494–497
17 Zhang L, Zheng D, Fan L, *et al.* Controllable ferromagnetism in super-tetragonal $PbTiO_3$ through strain engineering. Nano Lett, 2020, 20: 881–886
18 Sun DR, Xu GL, Zhang BB, *et al.* Implementation of ultrafast X-ray diffraction at the 1W2B wiggler beamline of Beijing Synchrotron Radiation Facility. J Synchrotron Rad, 2016, 23: 830–835

Acknowledgements This work was supported by the National Key Research and Development Program of China (2018YFA0703700 and 2017YFE0119700), the National Natural Science Foundation of China (21801013, 1190524, 51774034 and 51961135107), Beijing Natural Science Foundation (2182039), the Fundamental Research Funds for the Central Universities (FRF-IDRY-19-007 and FRF-TP-19-055A2Z), and the Young Elite Scientists Sponsorship Program by CAST (2019-2021QNRC). Use of the Beijing Synchrotron Radiation Facility (1W2B, 1W1A and 4B9B beamlines, China) of the Chinese Academy of Sciences is acknowledged.

Author contributions Zhang L designed and engineered the samples; Zhang B and Sun D designed the experiments; Zhang L, Zhang B and Chai M performed the data analysis; Zhang L and Zhang B wrote the manuscript with support from Tian J; Xing X, Chen J, and Tian J supervised the work and revised the manuscript. All authors contributed to the general discussion.

Conflict of interest The authors declare that they have no conflict of interest.

Linxing Zhang received his PhD degree in 2017 from the University of Science and Technology Beijing (USTB), and then joined the Institute for Advanced Materials and Technology in USTB. His research interest includes the design of functional thin films, structural analysis of epitaxial thin films, and ferroelectric and optoelectronic thin films. He won the China Outstanding Science and Technology Persons' Outstanding Impact Award and Young Elite Scientists Sponsorship Program awarded by the China Association for Science and Technology.

Darui Sun works at the Institute of High Energy Physics (IHEP), Chinese Academy of Sciences. She received her PhD degree from the University of Chinese Academy of Sciences in 2009. Her current research interest focuses on the time-resolved X-ray technology.

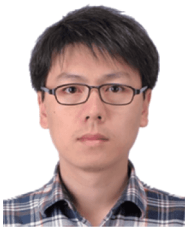

Bingbing Zhang received his PhD degree from the University of Chinese Academy of Sciences in 2016. After two years of Postdoc research at the IHEP, he has worked as a full-time employee of this institute and joined the High Energy Photon Source (HEPS) group in 2018. His current research interests focus on the development of ultrafast X-ray techniques and their application in the dynamic processes upon compression science and during the additive manufacturing. He is also responsible for the beamline design of the Structural Dynamic Beamline of HEPS.

Jianjun Tian received his PhD degree in 2007 from the USTB. During 2011–2012, he studied at the University of Washington. He was selected as new century excellent talents of the Ministry of Education in 2013, and built the Laboratory of Optoelectronic Materials and Devices in 2016 as leader (PI). He was nominated as director of the Functional Materials Institute, USTB in 2015 and vice-dean of the Institute for Multidisciplinary Innovation, USTB in 2019. Current research focuses on quantum dots and perovskites, and their applications, including solar cells, light emitting and photodetectors.

超四方相钛酸铅铁电薄膜的超快光致应变

张林兴[1†*], 孙大睿[2†], 柴茂盛[3], 邢献然[4], 陈骏[5], 张兵兵[2,6*], 田建军[1*]

摘要 近十年来, 由压电效应和光电效应进行铁电耦合的超快光致应变一直是人们关注的焦点. 这使得超快光致应变在超快光存储器、应变工程传感器和制动器等领域呈现出广泛的应用前景. 在铁电材料中, 光致载流子屏蔽去极化场被普遍认为是超快光致应变的机理, 而热应变通常被作为偏移误差而被忽视, 尚未得到系统研究, 导致不必要的混淆. 本文利用高重复率超快X射线衍射研究了复合外延铁电薄膜的正、负热膨胀效应, 同时考虑了压电效应和光伏效应. 在超快应变中, 正/负热效应和压电/光伏效应的耦合得到证实和调控. 在不同轴比的样品中, 由于热效应的不同, 晶格响应呈现相反的状态. 其最大超快光致应变可达0.24%, 与传统铁电的光致应变相当. 热效应和铁电效应在诱导应变中的相互作用可以促进光、热、电耦合的多样化应用.

